Comprehensive Optical Monitoring of Selective Laser Melting

M. Doubenskaia[1], M. Pavlov[1,2], S. Grigoriev[2], E. Tikhonova[2], I. Smurov[1]

[1] *Université de Lyon, Ecole Nationale d'Ingénieurs de Saint Etienne (ENISE), DIPI Laboratory, 58 rue Jean Parot, 42023 Saint-Étienne Cedex 2, France*
[2]*Moscow State Technological University "Stankin", Vadkovsky per., 1, 127994 Moscow, Russia*

The absence of on-line monitoring and process quality assurance is one of the main obstacles for wide implementation of Selective Laser Melting technology in modern manufacturing industry. Temperature monitoring in the laser impact zone are carried out by an originally developed bi-colour pyrometer and CCD camera which are integrated with the optical scanning system of the PHENIX PM-100 machine. Experiments are performed with variation of basic process parameters such as powder layer thickness (0-120 μm), hatch distance (60 μm-1000 μm), and fabrication strategy (the so-called "one-zone" and "two-zone").

DOI: 10.2961/jlmn.2012.03.0001
Keywords: optical monitoring, selective laser melting, pyrometry, CCD camera, high temperature.

1. Introduction

Modern Selective Laser Melting (SLM) systems are intended for melting a wide range of powder materials with greatly different properties, including melting point. Therefore the technological windows (i.e. optimum values of laser power, beam scanning speed, powder layer thickness, etc.) are rather different for different powders. The fabrication of a part with complex form and relatively large size can continue during 10 - 20 hours without any information about work in progress and possible problems. Typically the SLM process is carried out in closed environment without optical access for diagnostic equipment.

SLM is a repetitive stepwise process [1-7] (fig. 1): (a) A thin layer of powder is spread over a building substrate; (b) a laser beam selectively scans and fuses powder reproducing cross-sections generated from a 3D CAD digital model; (c) after a cross-section is fused, the powder bed is lowered, a new layer of powder is applied on top, and the process is repeated. Superposition of multiple cross-sections ultimately results in the desired solid 3D object.

To obtain the required geometry and structure of an object throughout a long-time fabrication cycle, consistent SLM conditions must be applied [8]. While manufacturing a part,

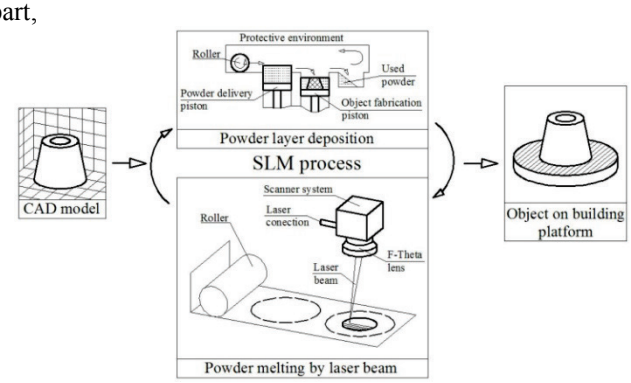

Figure 1. Repetitive basic stages of SLM technology: powder layering and laser beam scanning.

different modes of powder consolidation can occur even within a single layer owning to potential fluctuations in heat transfer process [9, 10]. As a result, different temperature cycles define different mechanical properties of the material, geometric accuracy and residual stresses.

The particular features of physical phenomena involved in SLM are related to strong modifications of heat and radiation transfer during powder melting by laser beam.

The thermal conductivity of a loose powder bed is an important material property in selective laser melting. The comparison of the experimental data with the model of discrete thermal resistances [11] indicates that the effective thermal conductivity of powder beds is proportional to the thermal conductivity of gas filling pores and also depends on the solid fraction and the particle size. For powders with particle size about several tens microns, the effective thermal conductivity is of the order of five to ten times the conductivity of air. Due to the large difference between the thermal conductivity of metals and air, the effective conductivity is mainly determined by the relative density of the powder bed and less by the properties of the powder material. In general, powder beds of irregular particles and of particles with a wide size distribution are more conductive than monodisperse spherical powders at the same density [11]. In the further discussion of the obtained results, one should remember that when there is a direct metallurgical contact between the laser remelted tracks, the heat flux through it could strongly contribute to the temperature evolution. On the contrary, heat transfer through powder bead is often negligible.

The laser radiation penetrates into the powder bed through an open pore system [12] and delivers energy directly to the powder bed volume and the substrate [13]. The radiative mechanism of energy transfer can be more important than the conductive one because of low thermal conductivity of powder [11], so that the spatial distribution of the deposited energy has a crucial effect on the local temperature field [13]. The principal questions arising at SLM concern the distribution of the incident laser energy between the back reflected radiation, the powder, and the

substrate; the uniformity of energy deposition in powder over the depth; and widening the energy deposition spot relative the incident laser beam. An important fraction of the laser energy absorbed directly by the substrate is favourable for formation of a metallurgical contact between the remelted powder and the substrate [13]. The depth and the width of the zone of laser energy release define the spatial resolution of SLM. Experimental studies of the reflection of the laser radiation by powder beds [14, 15] indicated that the absorptance of powder is considerably higher than the absorptance of the same material in the dense form.

The total absorptance of the system composed of a powder layer and a substrate of the same material on which the powder is deposited increases with the layer optical thickness and the absorptivity of the solid phase. The fraction of the incident radiation absorbed by the substrate decreases with the optical thickness of the covering powder layer and can have a local maximum as the function of the absorptivity of the solid phase [16]. The radial transport of the radiative energy due to scattering of the incident laser beam in the powder layer can considerably reduce the intensity of heat source at the centre of the beam. The widening of the radial profile of the deposited energy is less important. The whole energy efficiency of laser treatment and the heating of the substrate decrease with the reflectivity of the material. However, more uniform heating of the powder layer can be attained at higher reflectivity.

The basic objective of on-line process control in SLM is to assure quality of the developed parts and to optimise various stages of the process, for example to minimise the undesirable deviations from the required geometry and mechanical properties. To reach the goal, it is necessary to elaborate methodology and produce optical and electronic equipment for comprehensive process control using different and complementary diagnostic tools. “Integral” character of such system consists in the fact that it should monitor the whole sequence of manufacturing steps and inspects the built-up object throughout the entire manufacturing cycle. The integral process control/product quality inspection (IPC/PQI) system is intended:

- to set up optimal laser beam parameters prior to the manufacturing process;
- to control laser beam parameters in course of manufacturing;
- to permanently monitor quality of the powder layering;
- to examine the result of laser action onto the powder layer, i.e. fusion quality;
- to inspect on-line the built-up object in terms of geometric conformity, details accuracy.

The above mentioned objectives are realized only partly at present [17-21] and the paper is focused on application of a pyrometer and a CCD camera for monitoring of thermal processes in SLM and comparison of the results obtained by different diagnostic tools.

2. Experimental set-up

Non-contact optical methods are most suitable to reach the goal. It is supposed that the temperature value in the laser impact zone is rather sensitive to detect deviation of the SLM parameters from their optimums. For example, variations of the temperature and its instability will indicate that the energy input per unit length in the beam scanning strategy should be changed.

To exclude the influence of the scanning speed, observations must be carried out coaxially to the laser beam. In this case, for any position of the laser beam and for any scanning speed, the diagnostic system will register the signal from the processing zone.

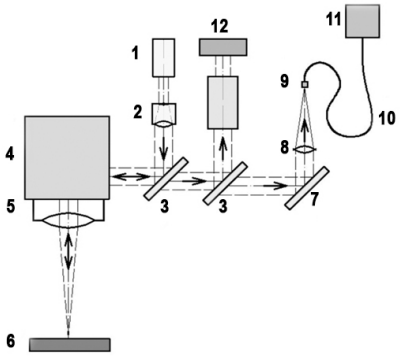

Figure 2. Schematic of the optical system applied: 1- fiber laser; 2 - beam expander; 3 - laser beam /thermal signal separating mirror; 4 - scanner head; 5 - F-Theta lens; 6 - powder bed; 7 - mirror; 8 - pyrometer lens; 9 - fiber tip; 10 - optical fiber; 11 - pyrometer; 12 - CCD camera.

In order to continuously monitor the surface temperature, i.e. temperature in the laser impact zone, a two-wavelength pyrometer (11, fig. 2) registering surface thermal radiation is connected to the optical unit by an optical fiber (10, fig. 2). In parallel, the CCD camera (12) measures thermal radiation from the heat affected zone (HAZ) that is much larger than the laser spot size.

3. Data acquisition

Pyrometer

Temperature was measured in the laser impact zone by an originally developed bi-colour pyrometer with the following performance: temperature range is 1200-2900 K, two InGaAs photodiodes with optical filters, transmission spectrum at central wavelength 1.26 μm with 100 nm bandwidth, 560 μm diameter of the zone of temperature measurements. The signal integration time is 50 ms with sampling time equals to 50 μs. At present, arbitrary units are used instead of the temperature values because of the following reasons: For correct pyrometric measurements, the zone of characteristic temperature variations must be larger than the pyrometer view field. In this study, the laser spot was 70 μm diameter that resulted in about 100-120 μm width of the remelted powder track. The 400 μm diameter optical fiber was used to avoid chromatic aberrations in the diagnostic system. Image magnification after passing through the optical system of the SLM machine (fig. 2): F - Theta lens (5), mirrors (3, 7) and pyrometer lens (8) is 1.4 times that provides the pyrometer observation zone of 560 μm diameter (fig. 3). That is why the results of pyrometric measurements for wavelength λ =1.26 μm are presented here in arbitrary units.

CCD camera

Brightness temperature distribution in the HAZ was acquired by the CCD camera (12, fig. 2) with a resolution of 560x760 pixels. The brightness temperature measurements were realized with the exposition time of 3 ms.

To obtain the brightness temperature, the CCD camera was calibrated using a W - halogen lamp with a transmitting diffuser. The W - halogen lamp was calibrated with a black body in the temperature range from 1200 to 1800 K.

Transversal and longitudinal profiles of brightness temperature captured by the CCD camera were obtained after treatment and averaging of 5 consecutive images. The values of brightness temperature used in figs. 6b, 10 correspond to the maximum temperature value in the heat affected zone.

For a further discussion, it is necessary to introduce a definition of a "track" and a "hatch distance". A track is the result of the laser beam scanning along a straight line on the powder bed with a constant speed. Hatch distance, δ, (fig. 4d) is the distance between the neighbour tracks.

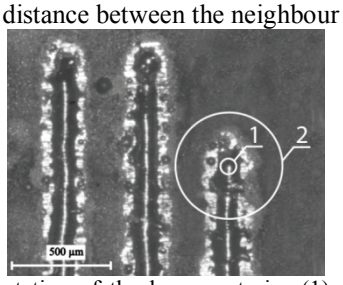

Figure 3. Presentation of the laser spot size (1) and pyrometer view field (2) on the remelted tracks.

To study the SLM thermal phenomena, a 10x10 mm^2 surface area was subjected to laser beam scanning. The scanning strategy is presented in fig. 4c: the scanning direction is the same within each layer. The tracks must be co-directional to avoid heat accumulation at their ends fig. 4c. The laser beam jumps between the consecutive tracks with a much higher speed ($7 \cdot 10^3$ mm/s) than the beam scanning speed (120 mm/s) during track formation.

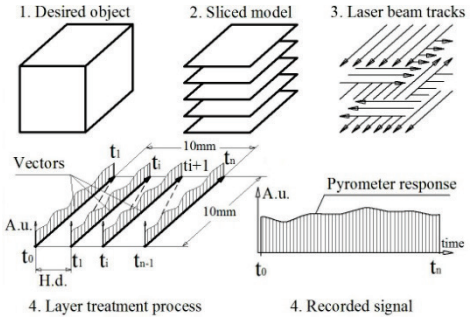

Figure 4. Principle of the pyrometer registering of the manufacturing process: t_0 and t_n are the start and end instants of the powder layer processing.

4. Process parameters

The experiments were carried out on Phenix PM100 machine (see SLM schematic in fig. 1). Laser source is YLR-50 a continuous wave Ytterbium fiber laser by IPG Photonics operating at 1075 nm wavelength with P = 50 W maximum output power.

In the present study, 32 W power was delivered to the powder layer. The laser spot size on the surface of the powder bed is 70 µm in diameter. Inox 304L 98 mm diameter plates are used as building substrates. The fabrication module provides a closed environment with protective atmosphere of pure nitrogen.

Unless otherwise stated, the following parameters were applied: laser beam scanning speed, v, is 120 mm/s, hatch distance, δ, is 120 µm, zone of beam scanning is a square 10x10 mm^2. Inconel 625 (-22 µm) powder was used.

5. Results and discussion

5.1 Laser scanning of steel substrate without powder Tables and illustrations

To illustrate the purpose of applying optical diagnostics for the SLM process, experiments were particularly aimed to register the superposition of thermal processes in the consequent tracks during laser scanning. A clean substrate of stainless steel with regular linear surface roughness R_a = 3.2 µm was used.

Consider heat processes during laser beam scanning of a rectangular. Duration of a single line (10 mm) scanned by the laser beam is 83.3 ms. During this time, the heat is spread over 660 µm (heat affected zone is estimated as $\sqrt{a \cdot (L/v)}$, where L is the track length, v is the beam scanning speed, and a is the temperature diffusivity of substrate) that is larger than the hatch distance (120 µm). That is why the next laser track will pass through the heat affected zone of the previous one. By superposition of the heat affected zones from a number of individual tracks, a macroscopic temperature field is formed with a maximum temperature close to the central part of the rectangular and lower temperature at its periphery. One may note the increase of the mean pyrometer signal with time in fig. 5. Indeed, after laser scanning, 10x10 mm^2 of substrate surface had 246 J energy input. Because of the chosen beam scanning strategy, all the tracks are started from one and the same side of the rectangular where temperature will be lower compared to the opposite side where tracks are finished. This is because of the transient period of heating at the beginning of each track. One can resume that the laser beam is crossing a non-uniform macroscopic temperature field which is superposed with its proper "microscopic" temperature field.

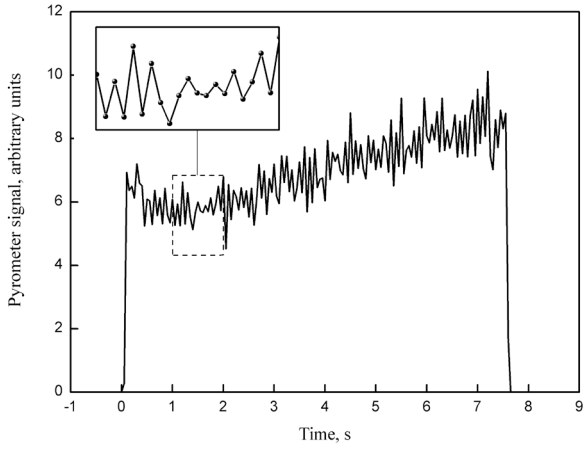

Figure 5. Pyrometer signal during laser beam scanning of a square area 10x10 mm^2 on steel substrate. Process parameters: scanning velocity v = 120 mm/s, incident laser power P = 32W, hatch distance δ = 120 µm.

The interval between consecutive temperature measurements (50 ms) is comparable with the time of a single line scanning (83 ms). This results in the following. Supposing that the current pyrometer measurement is done at the middle of the track (where contribution of the macroscopic temperature field is the highest), then the next measurement will be carried out 50 ms later that corresponds to about 8 ms after the beginning of the next line scanning (where contribution of the macroscopic temperature field is the lowest). As a result, the two consecutive measurements will provide different results. This is the reason of the oscillations of the pyrometer signal. One may note that the period of oscillations is close to 113 ms (results of Fourier analysis of the pyrometer signal) that corresponds to the double of the pyrometer sampling time. Indeed, if the current measurement is done somewhere in the middle of the track that provides "maximum" temperature, then the next measurement will be done at the beginning of the next track that will correspond to the "minimum" temperature, and the third measurement will be done about 60 ms after the beginning of the track scanning that one more time will provide "maximum" temperature.

5.2 Variation of hatch distance using thin powder layers

The hatch distance is one of the most significant parameter influencing the quality of the parts fabricated by SLM technology [3, 8]. Experiments were carried out with a 50 μm powder layer thickness and variation of the hatch distance, δ, from 70 μm up to 160 μm.

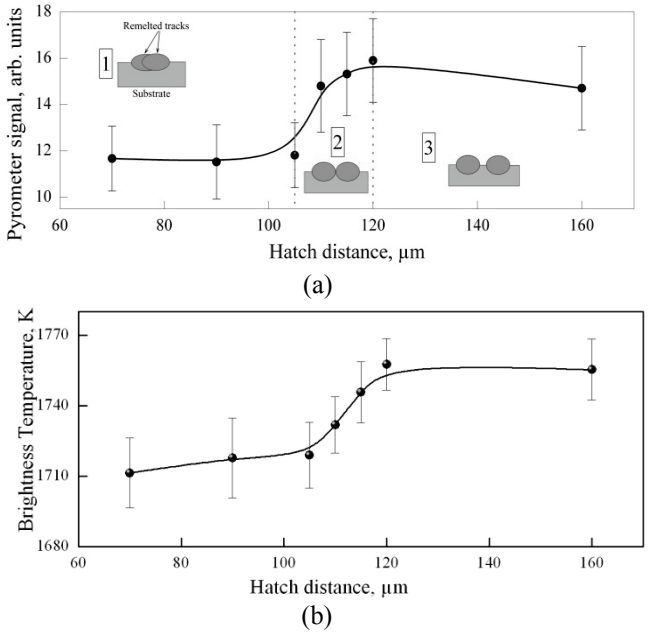

Figure 6. (a) - Variation of the pyrometer signal with hatch distance; (b) - variation of the maximum brightness temperature in HAZ measured by CCD camera with hatch distance. Process parameters: scanning velocity v = 120 mm/s, incident laser power P = 32W, powder layer thickness 50 μm; hatch distance, δ, varies from 70 μm up to 160 μm.

Several 10x10 mm^2 square areas were scanned by the laser beam using the same strategy as in chapter 5.1. The average value of the pyrometer signal and brightness temperature measured by CCD camera corresponding to the total scanning duration for one square were defined, as well as the range of deviations from the average value.

That is why each experimental point from fig. 6a,b corresponds to the scanning of the same square but with different hatch distances.

The increase of the average pyrometer signal during square scanning, similar to the one presented in fig. 5, was not detected when powder was deposited on the substrate, that could be explained by lower heat input into the substrate because of the energy consumed for powder melting.

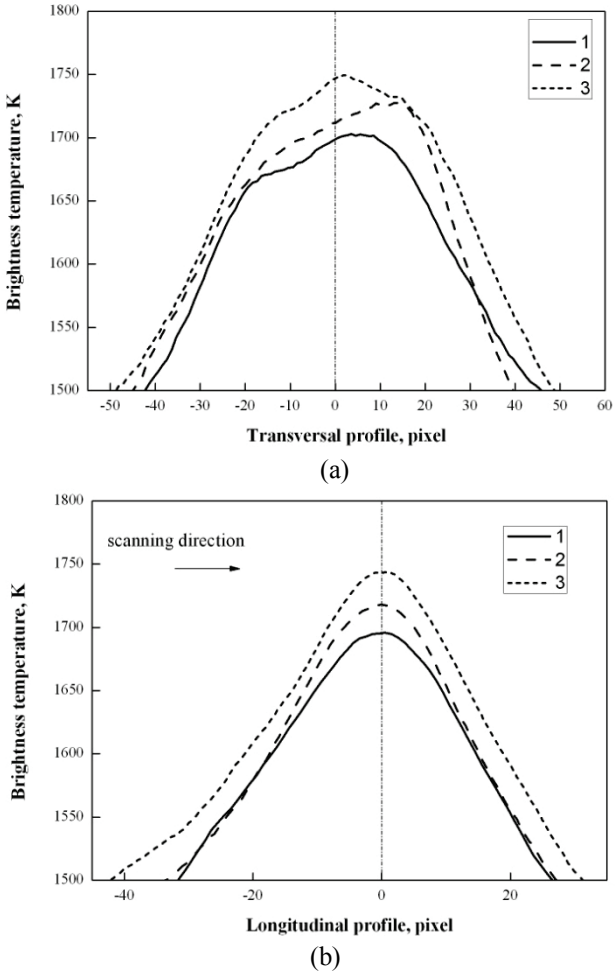

Figure 7. Influence of the hatch distance, δ, on brightness temperature measured by CCD camera: (a) – transversal temperature profile; (b) – longitudinal temperature profile. Curve *1* correspond to 70 μm hatch distance, *2* – 110 μm, *3* – 160 μm. Process parameters: scanning velocity v = 120 mm/s, incident laser power P = 32 W, powder layer thickness 50 μm.

In general, the temperature in the zone of laser action and the pyrometer signal depend on the heat loss into the substrate. That is determined by the contact area of the laser heated material and the cold substrate. Three zones can be distinguished in figure 6:

• In the first zone (δ is up to 105 μm), a consecutive track is so close to the previous one that they form direct metallurgical contact. The actual melt pool interacts with the previous track and the substrate resulting in significant heat losses. The transversal temperature profile width and the heat affected zone length are presented in fig. 7 a,b.

• The second zone (δ varies from 105 μm up to 120 μm) is characterized by the signal rise because the melt pool is no more in contact with the previously fabricated track. The volume of remelted powder increases with the

• In the third zone (δ is larger than 120 μm), interaction between the tracks is practically absent, and the volume of remelted powder per single track reaches maximum and constant value. Further slight decrease of the pyrometer signal with hatch distance is explained by lower energy input into the substrate when scanning the fixed surface of the squares by smaller number of laser tracks. The length and the width of the heat affected zone increases with hatch distance (curve 3 in fig. 7a,b).

5.3 Variation of the hatch distance using thick powder layers

10x10 mm^2 square on the surface of a 1 mm thick powder layer was scanned by the laser beam with hatch distance varying from 70 μm up to 1000 μm.

The particular feature of these experiments is that the tracks have no metallurgical contact with the substrate.

Surface structures presented in fig. 8 were fabricated by laser beam scanning of the 10x10 mm^2 square at the same conditions but different hatch distances δ. The scanning speed v = 120 mm/s, the laser power P = 32 W, and the layer thickness 1 mm were constant. Note that beam scanning direction was always the same, i.e. vertical, for all samples presented in fig.8.

For the entire ranges of the hatch distances, δ, applied, the first laser-scanned track results in separate spheres about 240 μm in diameter formed along the scanning direction. This phenomenon is driven by the Plateau–Rayleigh instability, often just called the Rayleigh instability, which provokes the disaggregation of the molten pool and the sphere formation under capillary force. For hatch distances δ = 300 μm and 1000 μm (Fig. 8e,f), zones of non-melted powder existed between the tracks, for example, the width of such zone was 60 μm for δ = 300 μm.

With the decrease of the hatch distance δ a contact appears between the track already melt in the form of separate spheres and the molten pool of the next track. In this case, the droplets of melted powder of the currently processed track stick to the spheres of the previous one. Thus, a structure perpendicular to the scanning direction is formed (Fig. 8a,b,c,d). This is a kind of self-organised surface structuring.

Evolution of the pyrometer signal versus hatch distance is presented in fig. 9.

The total scanning duration depends on the number of tracks which is defined by the hatch distance. This is why the durations of the thermal cycles in fig. 9 are different: the smaller the hatch distance, the greater is the number of tracks and the total duration of the scanning of 1cm^2.

Generally, increase of the pyrometer signal with the decrease of the hatch distance (Fig. 9) is the result of the difference in energy input into 1cm^2.

Thermal interaction between the tracks under the conditions of absence of metallurgical contact with the substrate could be described as follows:

• For the hatch distance less than 180 μm (fig. 7(a),(b),(c) and fig. 9 curves 4-6), the tracks are fused to one another forming a thin square object detaching from the substrate. At the beginning of the pyrometer registration, a significant increase of the signal is observed. This is caused by the heat accumulation in the previously fabricated tracks because of low heat loss into the surrounding powder layer. Further stabilization of the signal is related to the increase of the size of the fabricated object and an intensive heat transfer into it from the track under fabrication.

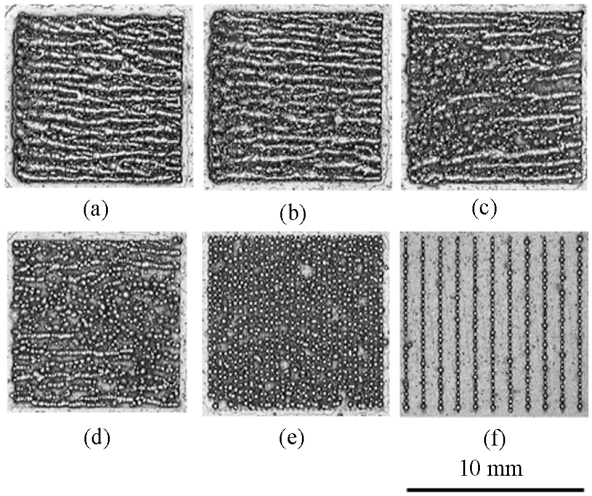

Figure 8. Photos of 10x10 mm^2 squares scanned by laser beam on a powder layer with different hatch distance: (a) – 70 μm; (b) – 90 μm; (c) – 120 μm; (d) – 180 μm; (e) – 300 μm; (f) – 1000 μm. Process parameters: scanning velocity v = 120 mm/s, incident laser power P = 32W, powder layer thickness 1 mm.

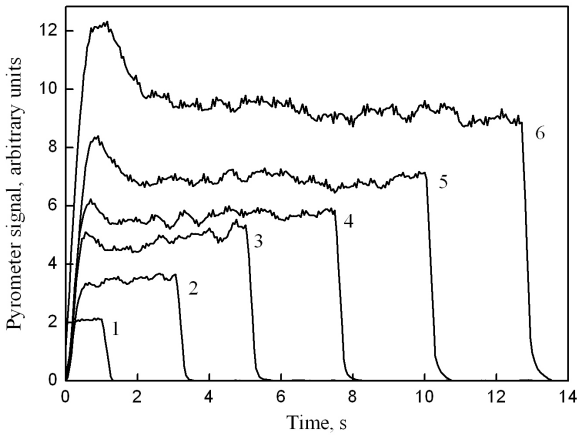

Figure 9. Evolution of the pyrometer signal versus hatch distance between consecutive tracks during scanning of one square centimeter. Thickness of the Inconel 625 powder layer is 1 mm. Curve *1* corresponds to the hatch distance equal to 1000 μm, *2* – 300 μm, *3* – 180 μm; *4* – 120 μm; *5* – 90 μm; *6* – 70 μm. Process parameters : scanning velocity v = 120 mm/s, incident laser power P = 32 W.

• In the case of the hatch distance from 180 μm up to 300 μm (fig. 8(d),(e) and fig. 9 curves 2,3), the neighboring tracks are separated by the powder. The pyrometer signal is stable during the whole laser scanning cycle. The heat transfer takes place through the powder situated in between the individual tracks.

• For a large hatch distance δ = 1000 μm (fig. 8(f) and fig. 9 curve 1), the pyrometer signal represents the formation of individual tracks when no interaction between them occurs.

5.4 Variation of powder layer thickness

Powder layer thickness is another important technological parameter of SLM. Relatively small thickness (minimum 20 μm) results in high accuracy of fabrication but low productivity, and vice versa.

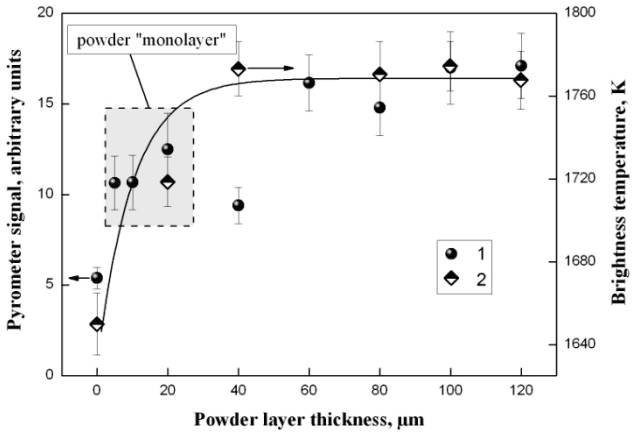

Figure 10. Variation of the pyrometer signal (1) and variation of the maximum brightness temperature in HAZ measured by CCD camera (2) with powder layer thickness. Process parameters: scanning velocity v = 120 mm/s, incident laser power P = 32W; hatch distance δ = 1 mm.

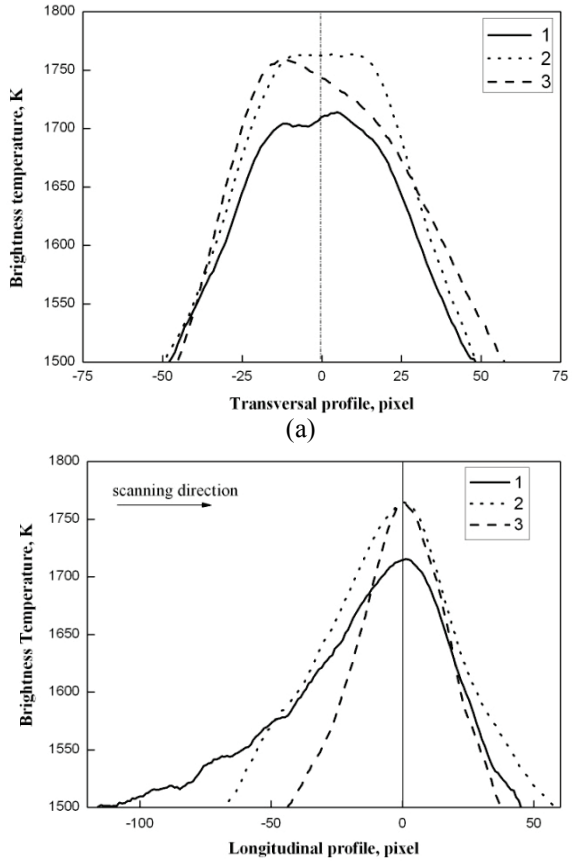

Figure 11. Influence of powder layer thickness on brightness temperature measured by CCD camera: (a) – transversal temperature profile; (b) – longitudinal temperature profile. Curve *1* correspond to 20 μm powder layer thickness, *2* – 40 μm, *3* – 120 μm. Process parameters: scanning velocity v = 120 mm/s, incident laser power P = 32W; hatch distance δ = 1 mm.

The increase of the pyrometer signal and maximum value of brightness temperature measured by CCD camera in the HAZ with powder layer thickness (figs. 10,11) is the result of the energy balance between powder melting and heat loss into the substrate (or a previously fabricated layer). For small powder layer thickness, important fraction of laser energy is spent on a substrate melting. Keeping in mind particle size distribution (< 20 μm), one may note that it is difficult to guarantee the uniform powder layer thickness in the range 10-20 μm. Most probably the results of temperature measurements are influenced by this fact.

It is known that the coefficient of thermal conductivity of a powder bed is 20 times lower than that of bulk material [12]. That is why the mean temperature grows with the powder bed thickness. Starting from a certain critical value the pyrometer signal and brightness temperature reaches the maximum and stable value because the contact between melted powder layer and the substrate is lost, and, thus, all the laser energy is absorbed by powder, and there are no heat losses into the substrate (fig. 10).

5.5 Monitoring during parts manufacturing: Influence of manufacturing strategy

Three different parallelepipeds (10x10x3 mm^3) were fabricated by applying three different manufacturing strategies, totally 57 powder layers were melted.

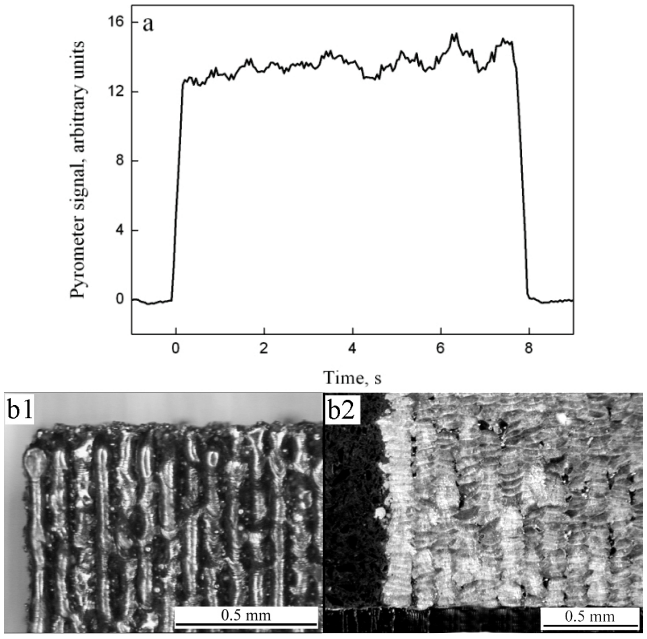

Figure 12. (a) - Evolution of the pyrometer signal for the 57th layer fabrication using the one-zone strategy; (b) - photos of the fabricated object: the 57th layer top views (b1) and cross-section (b2). Process parameters: scanning velocity v = 120 mm/s, incident laser power P = 32W; hatch distance δ =120 μm; 50 μm powder layer thickness.

The first strategy was the so-called "one-zone" technique (fig. 12 b1,b2). Each powder layer is processed by unidirectional laser beam passes with 120 μm hatch distance that is equal to the track width. The laser beam acts only on the currently processed powder layer without affecting the previously fabricated tracks. Objects thus fabri-

cated show vertical column-like structure. Regular vertical oriented zones with high porosity are easily seen.

The second strategy is the so-called "two-zone" technique (fig. 13b1, b2).

Each powder layer is processed in two steps: (1) first, the powder layer is processed with a hatch distance equal the average width of the vector which is about 120 μm for the applied powders and process parameters; (2) the laser beam passes in between the melted tracks of the same layer thus remelting no powder but two neighboring tracks previously fabricated (fig. 13b2). By this strategy, similar column-like structures are produced but with less porosity.

The sample surface is more homogeneous. Evident decrease of the pyrometer signal (fig. 13a) when the laser beam remelts the tracks without powder is observed.

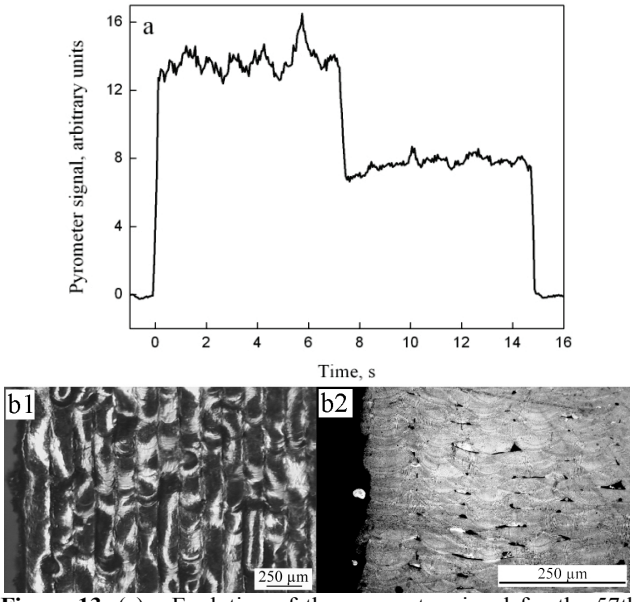

Figure 13. (a) - Evolution of the pyrometer signal for the 57th layer fabrication using the two-zone strategy; (b) - photos of the fabricated object: the 57th layer top views (b1) and cross-section (b2). Process parameters: scanning velocity v = 120 mm/s, incident laser power P = 32W; hatch distance δ = 120 μm; 50 μm powder layer thickness.

The third applied strategy is also "one-zone" technique (fig. 14b1,b2): each powder layer is processed by one pass but with 60 μm hatch distance. In this case, the laser beam melts simultaneously the previous track as well as the powder layer. The level of the pyrometer signal is lower than in fig. 12 because of the energy losses onto the previous tracks remelting.

For all the three strategies applied, the laser beam scanning speed and the powder layer thickness are identical. The first vector is processed under the same conditions in all of them. One may note that the pyrometer signals corresponding to the fabrication of these first tracks are also similar. That is why in fig. 14a the signal from the first track is higher than from the resting ones.

Different melting conditions in the "one-zone" and "two-zone" techniques result in different thermal cycles of powder consolidation, different solidification conditions, resulting structure and porosity (figs. 12-14). On-line control can ensure stability of the output parameters throughout the entire production process.

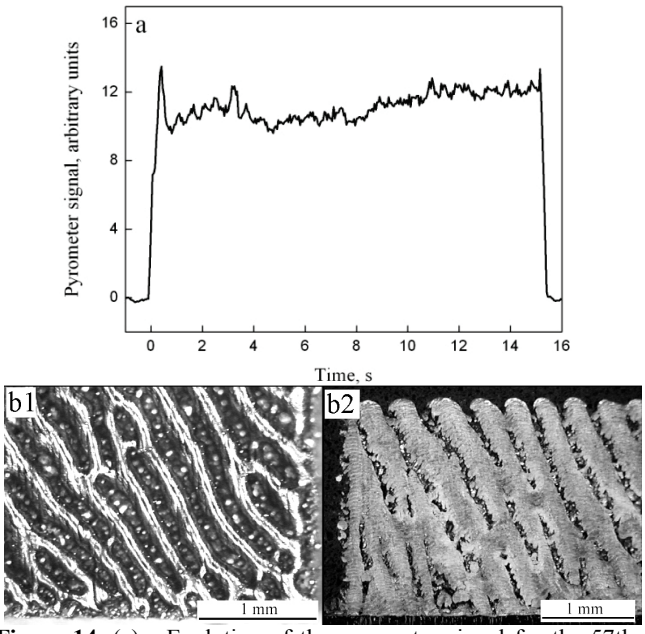

Figure 14. (a) - Evolution of the pyrometer signal for the 57th layer fabrication using one-zone strategy; (b) - photos of the fabricated object: the 57th layer top views (b1) and cross-section (b2). Process parameters: scanning velocity v = 120 μm/s, incident laser power P = 32W; hatch distance δ = 60 μm; 50 μm powder layer thickness.

6. Conclusions

The original optical diagnostic system was developed and integrated with commercial PHENIX PM-100 machine. It was found that the pyrometer signal from the laser impact zone and 2D temperature mapping from HAZ are rather sensible for variation of the main operational parameters (powder layer thickness, shift between consecutive laser beam passes, scanning velocity, etc.), and could be used for on-line control of manufacturing quality.

Variations of the pyrometer signal and brightness temperature with operational parameters were analyzed for the following cases:

• Variation of the hatch distance for 50 μm thickness powder layer (good metallurgical contact with substrate): Generally, the pyrometer signal increases with hatch distance. Three different zones of signal variation are found: (a) constant signal for low hatch distances (δ < 105 μm) when the consecutive track is so close to the previous one that they forme direct metallurgical contact; (b) constant signal for large hatch distances (δ > 120 μm) when the interaction between the tracks is practically absent, and the volume of remelted powder per single track reaches maximum value; (c) transition zone (105 μm < δ < 120 μm) where the pyrometer signal increases with hatch distance.

• Variation of the hatch distance for 1 mm thickness powder layer (no metallurgical contact with substrate): Generally, the pyrometer signal decreases with hatch distance. For the hatch distance less than 300 μm, a significant increase of the pyrometer signal at the beginning of the scanning is caused by heat accumulation in the previously fabricated tracks which are in direct metallurgical contact, and by low heat losses into the surrounding powder layer.

• Variation of the powder layer thickness: The increase of the pyrometer signal and the maximum brightness temperature in the HAZ with powder layer thickness from 20 μm up to 120 μm is the result of the energy balance between powder melting and heat losses into the substrate. Starting from a certain critical value, the pyrometer signal reaches the maximum and stable value because the contact between a melted powder layer and a substrate is lost, and thus, all the laser energy is absorbed by powder, and no heat losses into the substrate takes place.

Different melting conditions in the "one-zone" and "two-zone" techniques result in different thermal cycles of powder consolidation, different solidification conditions, resulting structure and porosity. The pyrometer signals differ as well, in particular, for the "two-zone" technique.

7. Acknowledgment

The work was supported by the Ministry of Education and Science of the Russian Federation (Decree 220).

References

[1]. M. Agarwala, D. Bourell, J. Beaman, H. Marcus and J.Barlow: Rapid Prototyping J., 1(1), (1995) 26. (Journals)
[2]. P.J.S. Bartolo et al.: "Virtual and rapid manufacturing" ed. by Taylor & Francis Group (London, 2008). (Books)
[3]. I. Yadroitsev: "Selective laser melting: Direct manufacturing of 3D-objects by selective laser melting of metal powders" ed. by Lap Lambert Acad. Publ., (Saarbüken, 2009). (Books)
[4]. T. Wohlers: "State of the industry, annual worldwide progress report" ed. by Wohlers Associates, Inc., (2008). (Books)
[5]. I. Yadroitsev, Ph. Bertrand, B. Laget, I. Smurov: J. Nucl. Mater., 362, (2007) 189. (Journals)
[6]. I. Yadroitsev, L. Thivillon, Ph. Bertrand, I. Smurov: Appl. Surf. Sci., 254 (4), (2007) 980. (Journals)
[7]. N.K. Tolochko, S.E. Mozzharov, I. Yadroitsev, T. Laoui, L. Froyen, V.I. Titov, M.B. Ignatiev : Rapid Prototyping J., 10 (2), (2004) 88. (Journals)
[8]. I. Yadroitsev, Ph. Bertrand, I. Smurov : Appl. Surf. Sci., 253 (19), (2007) 8064. (Journals)
[9]. A.V. Gusarov, I. Smurov: Appl. Surf. Sci., 255 (10), (2009) 5595. (Journals)
[10]. Y. Zhang, A. Fajhri: J. Heat Transfer, 120 (4), (1998) 883. (Journals)
[11]. M. Rombouts, L. Froyen, A.V. Gusarov, E.H. Bentefour, C. Glorieux: J. Appl. Phys., 97, (2005) 024905. (Journals)
[12]. A.V. Gusarov, J-P. Kruth: Int. J. Heat Mass Transfer, 48, (2005) 3423. (Journals)
[13]. A.V. Gusarov, I. Yadroitsev, Ph. Bertrand, I. Smurov: J. Heat Transfer, 131, (2009) 072101. (Journals)
[14]. N.K. Tolochko, T. Laoui, Yu.V. Khlopkov, S.E. Mozzharov, V. Titov, M.B. Ignatiev: Rapid Prototyping J., 6, (2000) 155. (Journals)
[15]. A.V. Gusarov, E.H. Bentefour, M. Rombouts, L. Froyen, C. Glorieux, J-P. Kruth: J Appl. Phys., 99, (2006) 113528. (Journals)
[16]. A.V. Gusarov, I. Smurov: J. Quantitative Spectrosc. Radiative Transfer, 111, (2010) 2517-2528. (Journals)
[17]. M. Doubenskaia, Ph. Bertrand, I. Smurov: Thin Solid Films, 453 – 454C, (2003) 477–485. (Journals)
[18]. J.-P. Kruth, J. Duffon, P. Mercelis et al.: Proc. of the LANE, ed. by M. Geiger, A. Otto, Erlangen, Germany, (2007) p.23. (Conference Proceedings)
[19]. I. Smurov: Proc. IV Int. WLT-Conf. on Lasers in Manufacturing, Munich, (2007) p.537. (Conference Proceedings)
[20]. M. Doubenskaia, Ph. Bertrand, H. Pinon, I. Smurov: Proc. IV Int. WLT-Conf. on Lasers in Manufacturing, Munich, (2007) p.547. (Conference Proceedings)
[21]. M. Doubenskaia, M. Pavlov, Yu. Chivel: Key Eng. Mater., 437, (2010) 458. (Journals)

(Received: June 06, 2011, Accepted: May 21, 2012)